ORIGINAL ARTICLE

Towards laser-induced fluorescence of nitric oxide in detonation

K. P. Chatelain[1,2] · S. B. Rojas Chavez[1,2] · J. Vargas[1,2] · D. A. Lacoste[1,2]

Abstract

This study aims to validate the new developments in our in-house spectroscopic code (KAT-LIF) to perform NO-LIF simulations for detonation conditions, as well as evaluating the capabilities of the NO-LIF diagnostic for characterizing H_2-air detonations. This objective was achieved in several steps. First, our in-house spectroscopic tool, KAT-LIF, was updated to perform NO-LIF simulations by notably developing a database of NO(A-X) transitions, currently unavailable in conventional spectroscopic databases, as well as collecting and implementing species-specific line broadening, line shifting, and quenching parameters for NO-LIF. Second, the validation of KAT-LIF was performed by comparing the simulation results with pre-existing simulation tools (LIFSim and LIFBASE) and experimental NO-LIF measurements in a laminar CH_4-air flame and H_2-air detonation. The validation results present satisfactory agreement of KAT-LIF and other simulation tools (LIFBASE, LIFSim) with experimental results for several conditions. For example, less than 20% discrepancy between the simulated and experimental NO-LIF profiles is observed for stoichiometric H_2-air detonation, initially at 20 kPa and 293 K. Third, qualitative and quantitative capabilities of the NO-LIF technique for detonation characterization are discussed, which include: shock detection, induction zone length measurements, and quantitative number density measurements.

Keywords LIF · NO · KAT-LIF · ZND · LIFSim

1 Introduction

As a result of climate change and the transition to low-carbon energy, hydrogen-fueled detonation engines have regained interest because of the potential to achieve more efficient power generation with carbon-free fuels. Since the discovery of detonation, many studies were performed to characterize the propagation regime (stable vs. oscillatory mode) and characteristic parameters (e.g., cell sizes) in different experimental configurations, ranges of conditions, and fuels.

Historically, most of these studies were performed with relatively simple diagnostics (e.g., pressure sensors/ion probes, soot foils, chemiluminescence, or schlieren/ shadowgraphy), which are still commonly used nowadays [1–4]. In contrast, only a limited number of advanced diagnostics were employed [1, 5–9] (interferometry, OH-PLIF visualization, and Rayleigh scattering) for qualitative or quantitative characterization of the detonation front, as compared to the work done on subsonic flames. Part of the reason for the limited number of studies is the high-speed and high-pressure reactive flow associated with detonation waves, as well as the challenges related to the required high-spatial and high-temporal resolution.

A few research groups characterized the detonation structure with the OH-PLIF technique [6, 8, 10]. Despite the limitations of the OH-PLIF diagnostic, notably the strong laser absorption and the limited information far from

✉ K. P. Chatelain
karl.chatelain@kaust.edu.sa

S. B. Rojas Chavez
samirboset.rojaschavez@kaust.edu.sa

J. Vargas
joao.dacruzvargas@kaust.edu.sa

D. A. Lacoste
deanna.lacoste@kaust.edu.sa

[1] Mechanical Engineering Program, Physical Science and Engineering Division, King Abdullah University of Science and Technology (KAUST), Thuwal 23955-6900, Saudi Arabia

[2] Clean Combustion Research Center (CCRC), King Abdullah University of Science and Technology (KAUST), Thuwal 23955-6900, Saudi Arabia

the detonation front, these measurements enabled a better understanding of the detonation structure at various conditions. Recent studies employing the OH-PLIF technique [8, 11] showed that using a transverse laser orientation or selecting different excitation strategies can overcome some of these limitations. Recently, two-dimensional temperature measurements were performed by Grib et al. [12] by using two-color OH-PLIF in a square detonation channel. Similarly, Fugger et al. [13] and Hsu et al. [14] performed high-frequency visualization (i.e., 1 MHz) by OH-PLIF in a rotating detonation engine. Developing or applying new laser diagnostics to H_2-air detonation waves seems to be a promising way towards more phenomenological comprehension of H_2-air detonations.

Laser-induced fluorescence of nitric oxide (NO-LIF) is a powerful technique that enables to obtain quantitative measurements in both subsonic combustion [15] and hypersonic flow studies [16–18]. Recently, the first NO-LIF profiles were obtained in stoichiometric H_2-air detonations at 20 kPa with a 1000 ppm NO seeding level in order to validate the spectroscopic code KAT-LIF [19]. Later, 2000 ppm NO seeding was employed for induction zone length measurements in a stoichiometric H_2-air detonation at 18 kPa in [20] using the same NO-LIF technique.

This study is an extension of the work presented in [19] and aims to provide more technical details on both the experimental and the numerical aspects, as well as to further discuss the additional capabilities of the technique for characterizing detonation waves. The first part of the manuscript focuses on the validation of KAT-LIF, based on comparisons with experimental and numerical data in both a stoichiometric CH_4-air flame and a stoichiometric H_2-air detonation. The second part of the manuscript presents the additional qualitative and quantitative capabilities of the technique for H_2-air detonation characterization.

2 Numerical method

2.1 Description of KAT-LIF

In [8], we developed and validated an in-house spectroscopic code called KAT-LIF. The code was previously employed to simulate the evolution of the spectrally-resolved OH-LIF intensity along the beam path for a set of user-specified parameters (e.g., laser parameters, mixture composition, and thermodynamic conditions). For OH-LIF simulations, the code utilizes the spectroscopic parameters of the OH transitions available in HITRAN [21], as previously reported in [8, 10, 11]. Also, KAT-LIF has several built-in functions that make it more suitable compared to other existing tools [22–24]. For example, KAT-LIF uses as an input the one-dimensional (1D) simulated detonation profiles, where both

the mixture composition and the thermodynamic conditions are obtained, in order to compute important spectroscopic parameters (e.g., line shape, line shifting, quenching, laser self-absorption, or Boltzmann fractions). Such workflow makes the simulation of high spatially resolved systems, such as detonations, more practical to simulate compared to point simulation software. Note that other tools (e.g., LIFSim or LIFBase [22, 23]) or other modeling methods (e.g., two-, three-, or five-level models [25–27]) exist in the literature to simulate NO-LIF profiles. However, most of these alternative solutions have drawbacks, either due to the number of user-inputs required (e.g., species-specific broadening, shifting, or quenching coefficients, as well as line-specific parameters such as Einstein coefficients), to the 0D simulation modeling (e.g., point simulation input/output), or due to output formatting such as the built-in autoscale in LIFBASE. The NO database, provided in the Supplementary Material, enables to compile the line-dependent parameters in a single document, currently not accessible in any of the well-known spectroscopic database (HITRAN, HITEMP, etc.).

As further detailed in the next sections, KAT-LIF compiles a large range of species-specific line broadening, line shifting, and quenching parameters, which makes its applicability more versatile for detonation applications than simpler models or software.

In this section, we present the three main updates of KAT-LIF enabling the NO-LIF simulations. These updates are focused on: (a) building the NO database, (b) adding the NO quenching calculation, and (c) adding the NO pressure shifts.

2.1.1 Building the NO database

To the best of the authors' knowledge, none of typical spectroscopic databases reports detailed list of rovibrationaly-resolved NO(A-X) transitions with their associated spectroscopic parameters required in KAT-LIF simulations. Namely: the line position ν (in m^{-1}), the Einstein-A coefficients A (in s^{-1}), the spectral line strength (also called spectral line intensity in HITRAN) at 296 K S_{ref} (in m^{-1}/(molecule $\cdot$ m^{-2})), the upper (g', unitless) and lower (g'', unitless) state degeneracies (also called the statistical weights), and the lower-state energy of the transition E'' (also called $E0$). Note that the NO transitions currently reported in HITRAN/HITEMP mainly belong to the NO(X-X) transitions or to the visible/infrared spectrum. Such transitions are not of interest for the present NO-LIF application.

A NO(A-X) database was built as followed from the transitions listed in LIFBASE [22], according to the following procedure: all the transitions available in LIFBASE [22] were considered, among the following: upper vibrational levels $v' = 0-5$, lower vibrational levels $v'' = 0-21$, lower rotational levels $N'' = 0-80$, and including their hyper-

fine structures (i.e., F1 and F2 in the case of NO(A-X) transitions). The ν and A coefficients were directly obtained from table reading. The quantity E'' was obtained from simple energy conservation calculations using $E' = E'' + \nu$, where E' and E'' are the upper- and lower-state energy of the transition ν (in cm^{-1}) and ν is the transition wavenumber (in cm^{-1}). Note that E' and E'' were rescaled by setting the lowest E'' to 0, as performed in HITRAN [21]. The quantities g' and g'' were obtained from the hyperfine calculation presented in [28], which gives for NO(A-X) transitions $g_{F1} = (2 \times (J^{\star} - 0.5) + 1) \times g_s$ and $g_{F2} = (2 \times (J^{\star} + 0.5) + 1) \times g_s$, where g_{F1} and g_{F2} are the degeneracy for F1 and F2 level; the quantity $J^{\star}$ corresponds to any upper (J') or lower (J'') rotational level; the quantity g_s corresponds to the state-dependent weight for NO provided in [28]. The line intensity was computed according to the equation presented in [10] by using the isotope abundance from [21] and the NO partition function from [29]. As a result, the NO(A-X) database includes more than 100,000 transitions from 1,060,623 to 5,695,552 m^{-1} ($\approx 176 - 943$ nm), among the following upper and lower vibrational levels $v' = 0-5$ and $v'' = 0-21$, and lower rotational quantum number $N'' = 0-80$.

Such a very large spectroscopic database affects the simulation time and could be reduced without affecting the numerical accuracy. In fact, a large majority of the transition lines have an extremely marginal line strength (10^9 lower than the most intense ones) and are typically for high vibrational and rotational numbers. These transitions are *a priori* not of interest for NO-LIF application, as they lead to very low LIF signals compared to the strongest lines. Thus, a reduced database, composed of more than 10,000 transitions (i.e., $> 90\%$ reduction), was obtained by considering only the transitions with the most intense line strengths ranging from 10^{-30} to 10^{-18} cm^{-1}/(molecule $\cdot$ cm^{-2}). These transitions with high line strength include the following upper and lower vibrational levels $v' = 0-5$ and $v'' = 0-3$ and lower rotational quantum number $N'' = 0-62$. The reduced database does not affect the simulation performance, and thus, it was employed in all the KAT-LIF simulations to save computation cost. Further reduction of the database must be investigated with care and may be considered in future studies.

Both databases are structured according to one of the HITRAN export formats and is available in the Supplementary Material. Parameters that could not be determined, or that are not required for KAT-LIF simulations, are labeled as not determined (ND). Note that the database could be extended for NO(B-X), NO(C-X), and NO(D-X) transitions by using an analogous procedure.

2.1.2 NO quenching calculation

The collisional quenching rate of NO with other colliders i is computed with the following equation from Paul et al. [30]:

$$Q = \frac{P}{kT} \left(\frac{8kT}{\pi m_{NO}} \right)^{0.5} \sum x_i \left(1 + \frac{m_{NO}}{m_i} \right)^{0.5} \sigma_{Qi} \qquad (1)$$

where P and T are the pressure (in Pa) and temperature (in K), respectively; k is the Boltzmann constant (in J/K); m_{NO}, m_i, x_i, and σ_{Qi} are the mass of NO, the mass of the collider i, the mole fraction of i, and the collisional quenching cross section of the collider i, respectively; the temperature dependence of σ_{Qi} was obtained by Paul [30] for Ar, NO$_2$, N$_2$O, and NH; Tamura et al. [31] for H, H$_2$, OH, and CH$_4$; Settersten et al. [32] for CO$_2$, CO, NO, and C$_2$H$_2$; Settersten et al. [33] for O$_2$, H$_2$O, and N$_2$.

2.1.3 Line shape calculation update

The Voigt profile calculation remained unchanged from [8, 11]. For the Doppler broadening term, only the mass of the absorbing species (NO) had to be updated. For the collisional broadening, species with an existing 2γ coefficient is directly employed using the following expression:

$$\Delta\nu_c = \sum_i P_i 2\gamma_{T_{ref},i} \left(\frac{T_{ref}}{T} \right)^{n_i} \qquad (2)$$

where $\Delta\nu_c$ is the collisional broadening, P_i is the partial pressure of species i, $2\gamma_{T_{ref},i}$ is the 2γ coefficient of the colliding species i at the reference T_{ref}, n_i is the temperature exponent of the colliding species i; 2Γ and n_i were employed for N$_2$, Ar, H$_2$O, O$_2$, and NO, as reported in [34, 35]. The generalized expression used for OH in [8] is employed for the collisional broadening of all the other molecules.

2.1.4 Line shift updates

Similar to that done for OH [11], the pressure shift of the NO transition lines is computed by:

$$\nu_s = \nu + P \sum_i x_i \delta_{i,T_{ref}} \left(\frac{T_{ref}}{T} \right)^{m_i} \qquad (3)$$

where ν_s and ν are the shifted and the initial transitions (in m^{-1}); $\delta_{i,T_{ref}}$, and m_i are the shift coefficient (in m^{-1}/atm) of the species i at the reference temperature (T_{ref}) and the temperature exponent (no unit), respectively. The parameters $\delta_{i,T_{ref}}$, and m_i were obtained from [34, 35] for N$_2$, Ar, H$_2$O, and O$_2$. Despite the recent results from [36] for NO (X-X) transitions, the pressure shift for NO(A-X) is currently line independent, due to the absence of data for NO(A-X) transitions as suggested in [34, 35].

2.1.5 Other important considerations in KAT-LIF simulations

As already expressed in [8], KAT-LIF simulations do not take into account the camera efficiency or the effect of photon trapping, while the filter transmission (i.e., Semrock-LP0224R) is considered. To the best of the authors' knowledge, there is no clear evidence of the effect of photon trapping on both NO-LIF and OH-LIF visualization of detonations. In addition, the present NO-LIF measurements can be considered to be in an optically-thin regime, due to the low absorption cross sections of the targeted NO transitions and the fact that measurements are conducted in a 40-mm-wide rectangular channel at 20 kPa. These conditions should minimize the photon-trapping effects.

2.2 Steady detonation modeling

The Zel'dovich–von Neumann–Döring (ZND) simulations are performed with the shock module of Chemkin-Pro, as employed in [37, 38]. As demonstrated in [37], this reactor model has the same performance as the conventional steady detonation modeling tools, such as ZNDkin (see previous usage in [8, 11, 37, 39]) and the Shock and Detonation Toolbox [40]. The reaction model of Mével et al. [41] was employed for the ZND simulations of H_2-air mixtures. This model comprises 31 species and 193 reactions. The ZND simulation output was used as the input to KAT-LIF to model the NO-LIF signal evolution in the detonation reaction zone. Figures 1a and b present the effect of the NO addition (without and with NO addition shown as open symbols and solid lines, respectively) on the ZND profiles of a stoichiometric H_2-air detonation, initially at $P = 10$ kPa and $T = 293$ K, for 100 ppm and 1000 ppm NO addition, respectively. The absence of any effect on the cell width (λ) was demonstrated experimentally by Chatelain et al. [42] for 2000 ppm of NO. As there is no effect of the NO addition on the main parameters (i.e., temperature, pressure, and thermicity), the H_2-air-NO mixture can effectively be employed to characterize the H_2-air detonation. In addition, the NO quantity can be adjusted to improve the signal-to-noise ratio.

2.3 Validation procedure

The updated KAT-LIF code was validated with new measurements and by comparing the simulation results with previously developed simulation tools, such as LIFBASE [22] and LIFSim [23]. All the following NO-LIF results consider a frontal laser orientation (i.e., laser propagating in the opposite direction of the detonation, see [11]), and the fluorescence is in the linear regime. The validation was performed in two steps. First, the evolution of fluorescence intensity in a stoichiometric methane-air flame, initially at
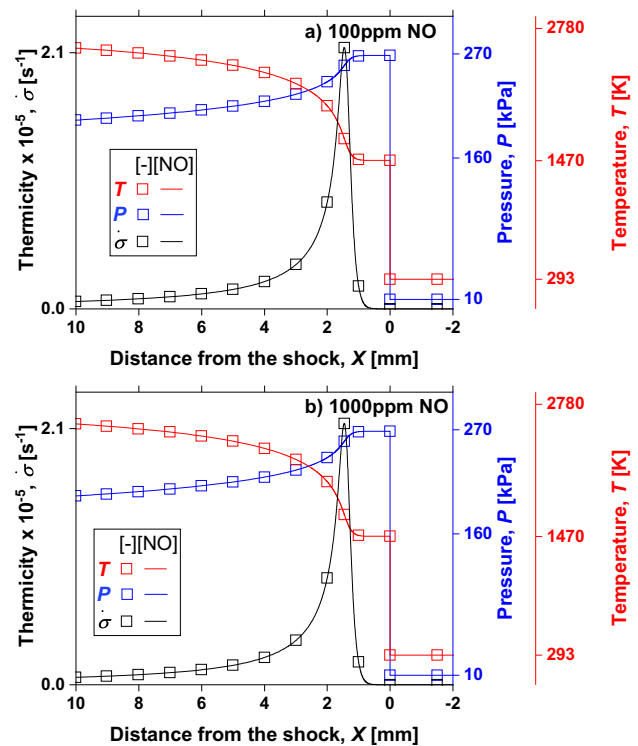

Fig. 1 Effect of a 100 ppm (**a**) and 1000 ppm (**b**) NO addition on the temperature (red), pressure (blue), and thermicity (black) profiles compared to a neat stoichiometric H_2-air detonation. The profiles without NO addition are shown as open symbols and the ones with NO correspond to the solid lines. Conditions are $P = 10$ kPa and $T = 293$ K

$P = 101$ kPa and $T = 293$ K, was compared between KAT-LIF, LIFBASE, LIFSim, and experimental results for different laser excitation wavelengths in the (0,0) and (0,1) bands. Second, the evolution of the fluorescence intensity in a stoichiometric H_2-air detonation, initially at $P = 10$–20 kPa and $T = 293$ K, was compared between KAT-LIF, LIFSim, and experimental results for a laser excitation wavelength at 225.120 nm, typically employed in flame diagnostics [43]. Note that the fluorescence intensity evolution in a detonation cannot be simulated with LIFBASE, due to the built-in autoscale. In addition to these validations, the line positions between LIFSim and KAT-LIF were compared in both the (0,0) and (0,1) bands and presented an average error of 0.3 and 0.4 pm with a maximum error of 0.5 and 0.6 pm, respectively.

3 Experimental procedure

3.1 Experimental setup

Experimentally, a 3-m-long optical detonation duct (ODD), same as [20], was employed to generate the H_2-air det-

onations. The main changes, with respect to the previous ODD [8], are briefly described in this section. The thickness of the channel was increased to 40 mm (i.e., $40 \times 17\,mm^2$ section) to enable the stable propagation of a stoichiometric H_2-air detonation, initially at $P = 20$ kPa and $T = 293$ K. Also, the visualization module and both the ignition source and the obstacle strategy (i.e., using meshes with a 200-mm pitch) were redesigned to suppress the detonation perturbation reported in [8] and to enhance the deflagration-to-detonation transition (DDT), respectively. To enable the NO-LIF diagnostic, the H_2-air mixture was seeded with 1000 ppm of NO by using a prediluted NO gas-cylinder (5000-ppm of NO in N_2). Equivalence ratio and mixture dilution was maintained by using a 50% oxygen-enriched air gas-cylinder (i.e., 50% O_2 in N_2). The NO concentration was selected based on numerical ZND simulation results (refer to the discussion of Fig. 1). The mixture preparation and ODD operating procedure remained unchanged from [8], enabling reproducible detonation experiments with low variability ($\pm 2\%$) in the initial pressure, equivalence ratio, NO concentration, or detonation speeds (D) near Chapman–Jouguet (CJ) conditions (i.e., $D/D_{CJ} \approx 1$). Note that no reactivity issues of the mixture were observed throughout this experimental campaign. This is attributed to the low initial pressure compared to [44] and the fact that premixtures were not employed.

The same slot burner as [8] was employed to perform the experimental laser scans and identify the laser excitation wavelength. A conventional stoichiometric methane-air flame was seeded with 1000 ppm of NO (similar to the detonation tests) to ensure a satisfactory signal-to-noise ratio.

3.2 Diagnostics

A conventional NO-LIF system was employed including: a Nd:YAG laser (Continuum Powerlite DLS9010) delivering a 7-ns pulse at 1064 nm with a 10-Hz repetition frequency; a dye laser (Continuum, ND6000) pumped by the frequency-doubled output of the Nd:YAG at 532 nm (≈ 740 mJ/pulse). Rhodamine 590 dye enables to reach ≈ 140 mJ near 566 nm. The laser beam at the output of the dye section was frequency doubled and mixed with the fundamental output of the Nd:YAG (i.e., 1064 nm) to obtain a laser excitation wavelength near 225 nm with a maximum energy output between 5–6 mJ/pulse and a laser spectral width of 8 pm. The laser excitation wavelength is determined before each set of measurements to mitigate a shift of a few pm in the grating angle calibration (i.e., displayed on the control unit of the ND6000). No changes were observed before and after a set of measurements. The selected laser excitation wavelength is $\lambda_{exc} = 225.120$ nm, exciting mainly the following NO A-X(0,0) transitions: R2(25.5), P21(29.5), Q1(29.5), Q2(31.5), and R12(31.5). The laser beam exiting the dye

laser at 225 nm was focused with a 1000 mm spherical lens into the slot burner, or the center of the visualization section of the ODD. The resulting beam diameter at focal point of the spherical lens, where the measurements are conducted, is near 0.7 mm. No significant variation of the laser fluence was observed within our field of view due to the long focal length employed to focus the beam. The linear regime of fluorescence was ensured by monitoring the fluorescence intensity evolution with the laser energy output.

The LIF signal was collected with an intensified-CCD camera (Princeton Instrument PI-MAX4, UV enhanced) equipped with a Nikon UV-lens (UV-Nikkor, 105 mm, f/4.5) and a long-pass filter (Semrock LP02-224R) with 90% transmission for most of the NO bands above 230 nm. This long pass filter enables the collection of OH* chemiluminescence in addition to the NO-LIF signal and NO chemiluminescence. The projected spatial resolution (or pixel density), near 40 μm, and the alignment with the laser were determined with a target. A 20-ns gate width, with maximum gain and low analog-to-digital conversion rate, was employed for the detonation experiment, while lower gain values were employed for the laser scans.

The synchronization between the laser, the camera, the ignition system, the acquisition system, and the detonation arrival was ensured with two pulse delay generators (BNC Model 575). First, the laser was warmed up for 10 min (i.e., 6000 pulses). Second, the last laser pulse (i.e., the 6000th pulse) was employed to trigger the ignition system. Then, the pressure sensors installed on the ODD were employed to synchronize the laser (i.e., flash lamp and Q-switch delay) with the camera opening and the detonation arrival in the field of view. All delays were adjusted to ensure a 10-Hz frequency between the 6000 pulses and the final pulse enabling the visualization.

3.3 Post-processing

The post-processing procedure employed for the detonation experiment is provided in Fig. 2. The raw single-shot NO-LIF images were background-corrected. Then, the LIF signal within the beam region (Area 1, in grey) was vertically-averaged to obtain a 1D profile. The OH* chemiluminescence contribution, extracted from the signal surrounding the laser beam (Area 2, in red), was removed to obtain the final NO-LIF profile. Similar post-processing procedure was followed for the laser scans, considering an accumulation of 20 numerical images in a 30 by 30 pixel square domain in the burnt gas region.

In the ODD experiment, the signal contamination was assessed by imaging the detonation without NO seeding to quantify the signal contamination throughout the 1D LIF profile. An average LIF signal contamination lower than 5% was observed after the shock with a maximum contamina-
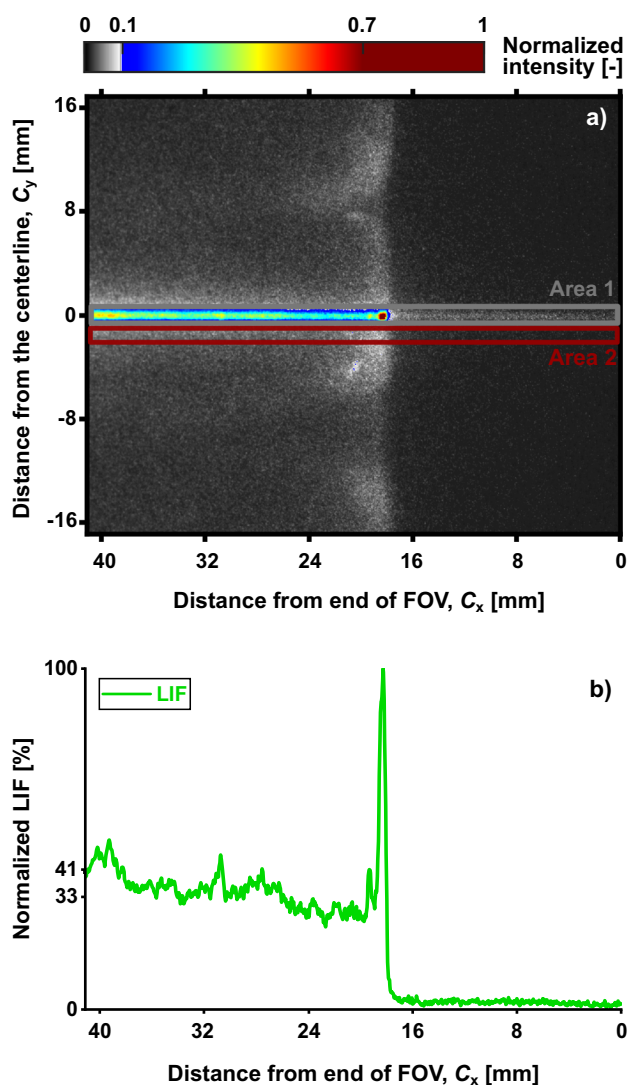
Fig. 2 Post-processing procedure from the background-corrected NO-LIF image. In **a**, the chemiluminescence (OH* + NO*) and NO-LIF are represented in gray and color scales, respectively. In **b**, the corrected 1D NO-LIF signal is obtained by subtracting the chemiluminescence contribution in Area 2 (red frame in **a**) into the raw LIF signal in Area 1 (grey frame in **a**)

tion near 8% of the LIF signal close to the shock (resulting from the OH* chemiluminescence mainly). In addition, O_2-LIF appeared negligible in the present conditions. Note that adding a short-pass filter to suppress the OH* chemiluminescence does not significantly modify the NO-LIF profile. Thus, a 5–10% uncertainty was estimated on the NO-LIF profile based on the distance from the shock.

A beam sampler and pyroelectric energy meter (Coherent J-25MB-LE) are installed on the beam path to record the energy of each pulse. All the NO-LIF profiles, obtained for both the laser scan and detonation experiments, are energy corrected.

4 Results and discussion

4.1 KAT-LIF validations

Laser scan validation Figure 3a and b present the fluorescence intensity evolution as a function of the laser excitation wavelength in the (0,0) and (0,1) bands, respectively. Figure 3a compares KAT-LIF, LIFSim, and experimental results obtained in the burned gases of a laminar premixed CH_4-air flame, initially at $T = 293$ K, $P = 101$ kPa, and $\phi = 1$. Note that the flame was seeded with 1000 ppm of NO to ensure a satisfactory signal-to-noise ratio. Figure 3b compares KAT-LIF, LIFSim, and LIFBASE results for the same conditions with a laser excitation wavelength in the (0,1) band. Note that only numerical validation of KAT-LIF was performed in the (0,1) band due to the experimental limitations of the Rhodamine 590 dye and the camera filter (Semrock LP02-224R) which cannot be employed for the (0,1) band. Figure 3a and b confirms the satisfactory agreement between the different simulations tools, and with experimental results, in terms of reproducing the fluorescence intensity evolution for atmospheric conditions ($P = 101$ kPa) and high temperature ($T \approx 2230$ K) for different laser excitation wavelengths. Also, these results indirectly validate the spectroscopic parameters calculated in the NO(A-X) database.

Detonation validation Numerical and experimental validations of KAT-LIF are demonstrated in Fig. 4a and b. Figure 4a presents a tailored validation case, based on a modified H_2-air ZND detonation profile, for which some input parameters were modified to facilitate the comparison between KAT-LIF and LIFSim simulation results. This tailored mixture had to be employed to mitigate some of the limitations of LIFsim, which does not consider important species for H_2 combustion such as H_2, OH, and H. Some of these species have significantly different quenching properties and thus strongly affect the simulated LIF signal. Note that: (i) the quenching parameters for Ar, H, H_2, OH, O_2, H_2O, N_2, NO_2, N_2O, NH, NO, CH_4, CO_2, CO, and C_2H_2 are considered in KAT-LIF; (ii) the NO concentration was fixed to 1000 ppm, as fixed in LIFSim; (iii) Doppler lineshift contribution was removed from KAT-LIF simulation, as Doppler lineshift is not considered in LIFSim; (iv) only CH_4, O_2, H_2O, and N_2 species are considered in both simulations to match the limited number of species in LIFSim. From Fig. 4a, a satisfactory agreement between KAT-LIF and LIFSim is observed with an average and a maximum discrepancy of 7% and 17%, respectively.
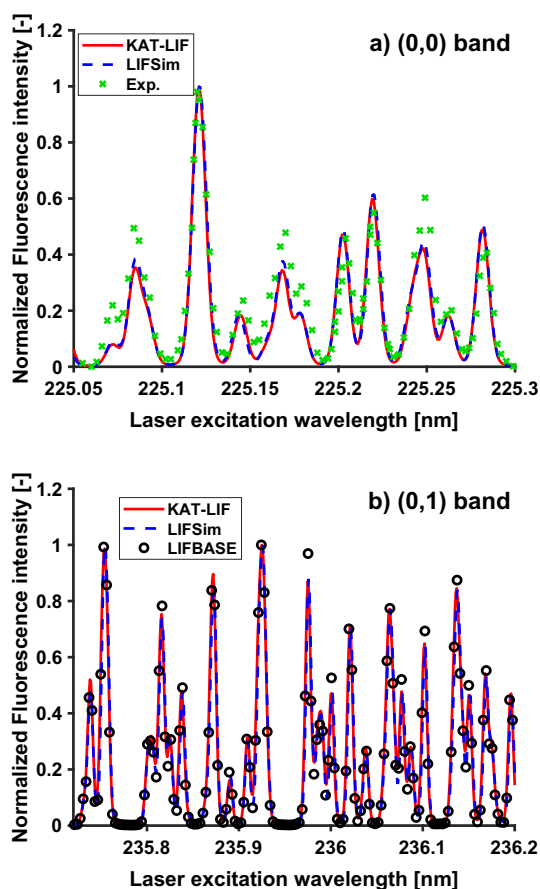
Fig. 3 Fluorescence intensity as a function of the laser excitation wavelength, including both experimental (Exp.) and simulation data (KAT-LIF, LIFSim, and LIFBASE), in the (0,0) and the (0,1) band in **a** and **b**, respectively. The conditions are: 8-pm FWHM laser width, $T = 2233$ K, $P = 101$ kPa, with the following major species: $x_{N_2} = 0.71$, $x_{CO_2} = 0.085$, and $x_{H_2O} = 0.18$. Note that LIFBASE results are not presented in **a** for clarity. Normalization is performed within each vibrational band
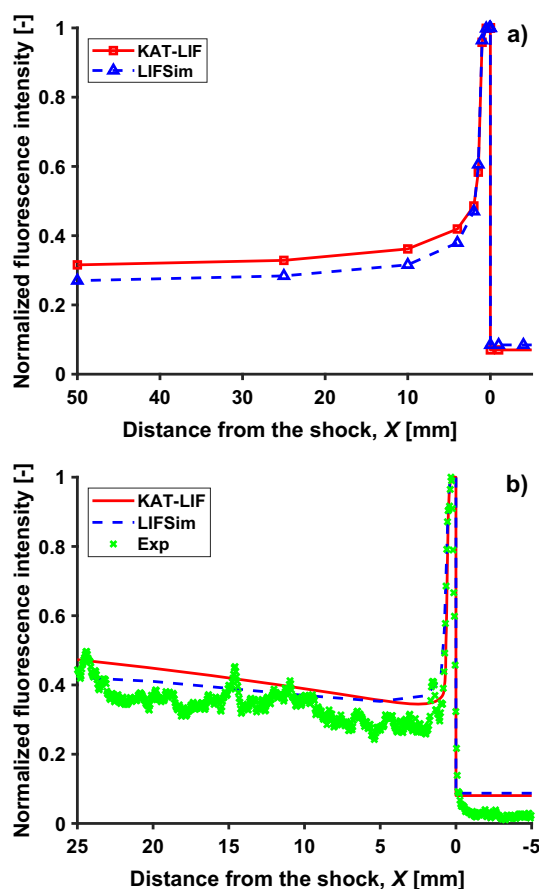
Fig. 4 Normalized NO fluorescence intensity as a function of the distance from the shock between KAT-LIF (red line) and LIFSim (blue symbol) in a tailored validation case (**a**) and in a real H_2-air detonation (**b**). Initial conditions are 10 and 20 kPa (in **a** and **b**, respectively) and 293 K. Note that H_2 is replaced by CH_4 in the LIFSim simulations. In **b**, the single-shot experimental result was selected such as $\Delta_{i,Exp} \approx \Delta_{i,ZND}$ and the ZND simulation at D_{CJ} was considered as an input of KAT-LIF and LIFSim simulations

The experimental (Exp) and simulated (KAT-LIF and LIFSim) fluorescence signal evolution as a function of the distance behind the shock for a H_2-air detonation, initially at $P = 20$ kPa, $T = 293$ K, and a 225.120-nm laser excitation wavelength are compared in Fig. 4b. As discussed previously in [20], the selected NO-LIF excitation wavelength is highly correlated with the NO number density evolution within the detonation wave, enabling to visualize the change in the thermodynamic conditions. The single-shot image, employed for this validation, was selected (i.e., such as the experimental Δ_i is near the theoretical value at D_{CJ} from ZND simulations) in order to have comparable thermodynamic conditions between the experiments and the ZND simulations. In fact, simulated NO-LIF profiles, obtained from KAT-LIF and steady ZND simulations at D_{CJ}, cannot be compared with single-shot imaging without considering

the variation of the shock wave strength through the detonation cell, as conducted in [20]. Satisfactory agreements are obtained for both KAT-LIF and LIFSim at reproducing the experimental profile with an average error near 20% and 10% in the reaction zone, respectively. Considering the variability of the LIF signal in the reaction zone, these low errors are within the experimental uncertainty of the NO-LIF experimental measurements. The differences in the NO-LIF profile between KAT-LIF and LIFSim can be mainly attributed to the simulation parameters listed in (b)–(d) of Sect. 2.1, as there are no detailed list of those species-specific parameters on the LIFSim webpage. Considering all the possible differences between the two codes (e.g., line positions or the broadening/shifting/quenching parameters), these small errors validate KAT-LIF and its NO(A-X) spectroscopic database.
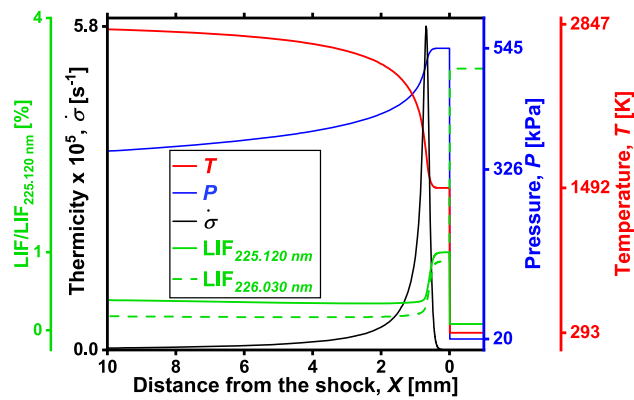
Fig. 5 The normalized LIF signal (LIF/LIF$_{225.120nm}$), thermicity ($\dot{\sigma}$), pressure (P), and temperature (T) profiles, where X is the distance from the shock. The NO-LIF profiles are obtained numerically from both 225.120- and 226.030-nm laser excitation wavelengths, from KAT-LIF simulations, using the experimental laser parameters (see Sect. 3). Conditions are H$_2$-air detonation, $\phi = 1$, 20 kPa and 293 K, and $x_{NO} = 1000$ ppm

4.2 Detonation structure determination

This section presents a few examples of the qualitative and quantitative capabilities of the NO-LIF technique for detonation characterization.

Shock detection capabilities As observed in the previous sections (see Figs. 2 and 4) and in [19, 20], the NO-LIF technique enables the identification of the shock location along the beam based on the post-shock NO fluorescence. Extended to 2D, the NO-PLIF diagnostic could provide a non-line-of-sight integrated technique, as opposed to the widely-employed schlieren/shadowgraphy techniques, to visualize the detonation shock wave location. This precise visualization of the front is even more beneficial for detonation diagnostics in non-canonical configurations, where the channel width (w) is much larger than the cell width ($w/\lambda >> 1$). A large number of excitation wavelengths could enable these shock detections with a satisfactory signal-to-noise ratio, comparable to the one presented in this study. Figure 5 presents, qualitatively from KAT-LIF simulations, two NO-LIF profiles obtained with 225.120 and 226.030-nm excitation wavelengths, respectively, for a NO-seeded stoichiometric H$_2$-air detonation at $P = 20$ kPa and $T = 293$ K (where X is the distance from the shock). The temperature (T), pressure (P), and the thermicity ($\dot{\sigma}$) profiles are also depicted in Fig. 5. A large number of laser excitation wavelengths exhibits a similar NO-LIF profile as for 225.120 nm, where the LIF signal is: low in the fresh gases, maximum in the von Neumann (vN) state, decreasing in the exothermic part/gas expansion, and increasing again due to the thermal NO produced in the reaction zone. Alternative NO-LIF profiles can also be observed, as for 226.030-nm excitation, where the LIF signal is: maximum in the fresh

gases, a first LIF signal reduction in the vN state, a second LIF signal reduction in the exothermic part/gas expansion, and a LIF signal increase due to the thermal NO produced in the reaction zone. Note that the maximum NO-LIF signal could be obtained far from the shock ($X >>> 100$ mm), where NO mole fraction is high.

Induction zone length measurements The capabilities of the NO-LIF technique at measuring the induction zone lengths in H$_2$-air detonation were demonstrated in [20] over a large range of conditions, using the 225.120-nm laser excitation wavelength by a single correlation (i.e., -84% of the LIF signal decay from the LIF maximum). This section aims to numerically verify the validity of the correlation proposed in [20] in the present conditions and the possibility to employ another laser excitation wavelength to measure induction zone length. As discussed in [20], the validity of this correlation must be extended with care to other laser excitation wavelengths or mixtures, due to different NO-LIF profile evolutions. In fact, the maximum of the LIF signal does not correspond to the vN state for a laser excitation wavelength of 226.030 nm. Nevertheless, a correlation of the LIF signal decay with the thermicity peak is still observed, which indicates that Δ_i can be determined. In fact, Δ_i is accurately determined from both laser excitation wavelengths by considering the -84% of the LIF signal decay from the vN state with the present experimental resolution. Note that employing -79% of the LIF signal decay with a CJ ZND simulation and an excitation wavelength of 226.030 nm significantly improves the accuracy of the Δ_i determination method. Extending the validity of this new correlation for the 226.030-nm laser excitation wavelength to a larger range of initial pressures and equivalence ratios is outside the scope of the study.

Quantitative NO measurements This section aims at assessing, numerically, the capabilities of NO number density (N_{NO}) measurements from the NO-LIF profile for H$_2$-air, $\phi=1$, $P=20$ kPa, and $T=293$ K and the methodology described in [8] using OH-LIF profiles. The relation between the NO number density ($N_{NO,ZND}$), obtained directly from ZND simulations, and the LIF signal (LIF), obtained from post-processing of the ZND simulation by KAT-LIF, is determined at two locations behind the shock. N_{NO,k_1} corresponds to the recalculated NO number density from the LIF signal, obtained from a single calibration constant, k_1, determined in the vN state: $k_1 = $ LIF$_{x=vN}$/NO$_{ZND,x=vN}$. N_{NO,k_2} corresponds to the recalculated NO number density from the LIF signal, obtained from a single calibration constant, k_2, determined at $x = 20$ mm behind the shock: $k_2 = $ LIF$_{x=20\,mm}$/N$_{NO_{ZND},x=20\,mm}$. Figure 6 presents the theoretical and recalculated NO number density profile, as well as the normalized LIF signal as a function of the distance from the shock. From Fig. 6, it is
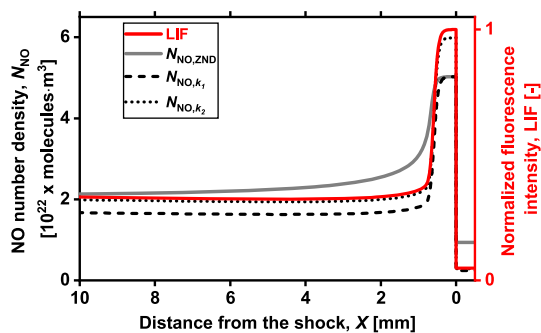
Fig. 6 Evolution of both the NO number density and the LIF signal as a function of the distance from the shock. The quantity $N_{NO,ZND}$ stands for the initial NO number density obtained from ZND simulations; N_{NO,k_1} and N_{NO,k_2} stand for the recalculated NO number density from the LIF signal using the calibration constant k_1 (x = vN) and k_2 (x = 10 mm). Conditions are H_2-air detonation, ϕ = 1, 20 kPa and 293 K, and X_{NO} = 1000 ppm

clear that none of recalculated NO number density accurately reproduces the theoretical $N_{NO,ZND}$ for all distances behind the shock. In fact, the error between the recalculated NO number density and $N_{NO,ZND}$ varies significantly for different distances behind the shock. For short distances ($0 < x < \Delta_i$) after the shock, an average error of 10% is obtained using k_1, while a larger error (18%) is obtained with k_2. For longer distances ($0 < x < 20$ mm) after the shock, an average error of 9% is obtained using k_2, while a larger error (22%) is obtained with k_1. In addition, maximum errors range between 36–46% for both k_1 and k_2, near the thermicity peak, and indicate the inability to use single-point calibration for quantitative NO number density measurements for the present conditions. As observed in [8] for OH, this is due to the strong thermodynamic changes across the detonation wave, which prevents the correlation of the LIF signal to the NO number density over a large range of conditions (e.g., from vN to CJ condition), as the NO number density, transition line shift, transition line broadening, and mixture quenching cannot be considered constant. Although no single calibration constant can be obtained for all distances after the shock, we note that a single calibration constant could be used to obtain an estimate of NO concentration in the burned gases since the thermodynamic conditions do not change abruptly far from the shock.

5 Conclusions

This study aimed at validating the developments in our in-house spectroscopic code, KAT-LIF, to perform NO-LIF simulations for H_2-air detonation conditions. This objective was achieved in two steps. First, KAT-LIF was updated to perform NO-LIF simulations by developing a database of

NO(A-X) transitions and updating a large range of species-dependent spectroscopic parameters (line broadening, line shifting, and quenching parameters for NO-LIF).

Second, the validation of KAT-LIF was performed by comparing the simulation results with other existing simulation tools and experimental NO-LIF measurements made for a laminar CH_4-air flame and H_2-air detonation. The validation results indicate: (i) the NO-LIF intensity evolution simulated by KAT-LIF was in agreement with experimental and other simulation tools (LIFBASE and LIFSim) results for different laser excitation wavelengths in a typical stoichiometric CH_4-air flame (atmospheric pressure and high temperature); (ii) both KAT-LIF and LIFSim satisfactorily reproduced the LIF intensity evolution in a stoichiometric H_2-air detonation. The small discrepancy observed between both codes and the experimental profile are mainly attributed to the experimental uncertainties; (iii) a numerical discrepancy of about 7% was observed between the KAT-LIF and LIFSim simulation results for a tailored validation case. This marginal difference is related to small differences in the codes (e.g., line positions, quenching parameters, line shifting, or line broadening), which cannot be identified precisely.

In addition, this study demonstrated the possibility to apply the NO-LIF technique with different laser excitation wavelengths for shock position and induction zone length measurements. However, it was demonstrated that quantitative NO number density measurements are not achievable from the NO-LIF profile and the use of a single calibration constant results in maximum errors as high as 36–46%. Future work will focus on obtaining more quantitative measurements for a H_2 detonation by using the NO-LIF technique and extending the presented results to 2D (NO-PLIF).

References

1. Shepherd, J.E.: Detonation in gases. Proc. Combust. Inst. **32**(1), 83–98 (2009). https://doi.org/10.1016/j.proci.2008.08.006
2. Frederick, M.D., Gejji, R.M., Shepherd, J.E., Slabaugh, C.D.: Time-resolved imaging of the cellular structure of methane and natural gas detonations. Shock Waves **32**, 337–351 (2022). https://doi.org/10.1007/s00193-022-01080-8
3. Melguizo-Gavilanes, J., Rodriguez, V., Vidal, P., Zitoun, R.: Dynamics of detonation transmission and propagation in a curved chamber: a numerical and experimental analysis. Combust. Flame **223**, 460–473 (2021). https://doi.org/10.1016/j.combustflame.2020.09.032

4. Gray, J.A.T., Lacoste, D.A.: Effect of the plasma location on the deflagration-to-detonation transition of a hydrogen-air flame enhanced by nanosecond repetitively pulsed discharges. Proc. Combust. Inst. **38**(3), 3463–3472 (2021). https://doi.org/10.1016/j.proci.2020.06.369

5. Lee, J.J., Dupré, G., Knystautas, R., Lee, J.H.: Doppler interferometry study of unstable detonations. Shock Waves **5**(3), 175–181 (1995). https://doi.org/10.1007/BF01435525

6. Pintgen, F., Eckett, C.A., Austin, J.M., Shepherd, J.E.: Direct observations of reaction zone structure in propagating detonations. Combust. Flame **133**(3), 211–229 (2003). https://doi.org/10.1016/S0010-2180(02)00458-3

7. Chacon, F., Gamba, M.: OH PLIF visualization of an optically accessible rotating detonation combustor. AIAA Propulsion and Energy 2019 Forum, Indianapolis, IN, AIAA Paper 2019-4217 (2019). https://doi.org/10.2514/6.2019-4217

8. Rojas Chavez, S.B., Chatelain, K.P., Guiberti, T.F., Mével, R., Lacoste, D.A.: Effect of the excitation line on hydroxyl radical imaging by laser induced fluorescence in hydrogen detonations. Combust. Flame **229**(3), 111399 (2021). https://doi.org/10.1016/j.combustflame.2021.111399

9. Boeck, L.R., Lapointe, S., Melguizo-Gavilanes, J., Ciccarelli, G.: Flame propagation across an obstacle: OH-PLIF and 2-D simulations with detailed chemistry. Proc. Combust. Inst. **36**(2), 2799–2806 (2017). https://doi.org/10.1016/j.proci.2016.06.097

10. Mével, R., Davidenko, D., Austin, J.M., Pintgen, F., Shepherd, J.E.: Application of a laser induced fluorescence model to the numerical simulation of detonation waves in hydrogen-oxygen-diluent mixtures. Int. J. Hydrog. Energy **39**(11), 6044–6060 (2014). https://doi.org/10.1016/j.ijhydene.2014.01.182

11. Chatelain, K.P., Mével, R., Melguizo-Gavilanes, J., Chinnayya, A., Xu, S., Lacoste, D.A.: Effect of incident laser sheet orientation on the OH-PLIF imaging of detonations. Shock Waves **30**, 689–702 (2020). https://doi.org/10.1007/s00193-020-00963-y

12. Grib, S.W., Fugger, C.A., Hsu, P.S., Jiang, N., Roy, S., Schumaker, S.A.: Two-dimensional temperature in a detonation channel using two-color OH planar laser-induced fluorescence thermometry. Combust. Flame **228**(1), 259–276 (2021). https://doi.org/10.1016/j.combustflame.2021.02.002

13. Fugger, C.A., Hsu, P.S., Jiang, N., Roy, S., Slipchenko, M., Athmanathan, V., Webb, A., Fisher, J., Meyer, T.R.: Megahertz OH-PLIF imaging in a rotating detonation engine. AIAA Scitech Forum, Virtual Event, AIAA Paper 2021–0555 (2021). https://doi.org/10.2514/6.2021-0555

14. Hsu, P.S., Slipchenko, M., Jiang, N., Fugger, C.A., Webb, A.M., Athmanathan, V., Meyer, T.R., Roy, S.: Megahertz-rate OH planar laser-induced fluorescence imaging in a rotating detonation combustor. Opt. Lett. **45**(30), 5776–5779 (2020). https://doi.org/10.1364/OL.403199

15. Wang, G., Tang, H., Yang, C., Magnotti, G., Roberts, W.L., Guiberti, T.F.: Quantitative laser-induced fluorescence of NO in ammonia–hydrogen–nitrogen turbulent jet flames at elevated pressure. Combust. Flame (2022) (**in press**). https://doi.org/10.1016/j.proci.2022.08.097

16. McDougall, C.C., Johansen, C.T., Herrmann-Stanzel, R., Danehy, P.M., Splinter, S.C., Gragg, J.G.: Nitric oxide laser-induced fluorescence rotational thermometry in a hypersonic non-equilibrium flow. AIAA Scitech 2020 Forum, Orlando, FL, AIAA Paper 2020–920 (2020). https://doi.org/10.2514/6.2020-0920

17. McDougall, C.C., Hinman, W.S., Johansen, C.T., Bathel, B.F., Inman, J.A., Danehy, P.M.: Evaluation of nitric oxide laser-induced fluorescence thermometry techniques in a hypersonic boundary layer. Exp. Fluids **61**, 102 (2020). https://doi.org/10.1007/s00348-020-2884-1

18. Matos, P.A.D.S., Barreta, L.G., Martins, C.A.: Velocity and NO-lifetime measurements in an unseeded hypersonic air flow. J. Fluids Eng. **140**(12), 121105 (2018). https://doi.org/10.1115/1.4039863

19. Chatelain, K.P., Rojas Chavez, S.B., Vargas, J., Lacoste, D.A.: Towards laser-induced fluorescence of nitric oxide in detonation. 28th International Colloquium on the Dynamics of Explosions and Reactive Systems, Naples (Italy), Paper 164 (2022)

20. Rojas Chavez, S.B., Chatelain, K.P., Lacoste, D.A.: Induction zone length measurements by laser-induced fluorescence of nitric oxide in hydrogen-air detonations. Proc. Combust. Inst. (2022). https://doi.org/10.1016/j.proci.2022.09.020 (**In press**)

21. Gordon, I.E., Rothman, L.S., Hill, C., Kochanov, R.V., Tan, Y., Bernath, P.F., Birk, M., Boudon, V., Campargue, A., Chance, K.V., Drouin, B.J., Flaud, J.-M., Gamache, R.R., Hodges, J.T., Jacquemart, D., Perevalov, V.I., Perrin, A., Shine, K.P., Smith, M.-A., Tennyson, J., Toon, G.C., Tran, H., Tyuterev, V.G., Barbe, A., Császár, A.G., Devi, V.M., Furtenbacher, T., Harrison, J.J., Hartmann, J.-M., Jolly, A., Johnson, T.J., Karman, T., Kleiner, I., Kyuberis, A.A., Loos, J., Lyulin, O.M., Massie, S.T., Mikhailenko, S.N., Moazzen-Ahmadi, N., Müller, H., Naumenko, O.V., Nikitin, A.V., Polyansky, O.L., Rey, M., Rotger, M., Sharpe, S.W., Sung, K., Starikova, E., Tashkun, S.A., Auwera, J.V., Wagner, G., Wilzewski, J., Wcisło, P., Yu, S., Zak, E.J.: The HITRAN2016 molecular spectroscopic database. J. Quant. Spectrosc. Radiat. Transfer **203**, 3–69 (2017). https://doi.org/10.1016/j.jqsrt.2017.06.038

22. Luque, J.: LIFBASE, Database and spectral simulation for diatomic molecules. SRI International Report 99 (1999)

23. Bessler, W.G., Schulz, C., Sick, V., Daily, J.W.: A versatile modeling tool for nitric oxide LIF spectra. Proceedings of the Third Joint Meeting of the US Sections of The Combustion Institute, Chicago, IL, Paper P105 (2003)

24. Foo, K.K., Lamoureux, N., Cessou, A., Lacour, C., Desgroux, P.: The accuracy and precision of multi-line NO-LIF thermometry in a wide range of pressures and temperatures. J. Quant. Spectr. Radiat. Transfer **255**, 107257 (2020). https://doi.org/10.1016/j.jqsrt.2020.107257

25. Watson, G.M.G., Versailles, P., Bergthorson, J.M.: NO formation in premixed flames of C1–C3 alkanes and alcohols. Combust. Flame **169**, 242–260 (2016). https://doi.org/10.1016/j.combustflame.2016.04.015

26. Durocher, A., Meulemans, M., Versailles, P., Bourque, G., Bergthorson, J.M.: Back to basics - NO concentration measurements in atmospheric lean-to-rich, low-temperature, premixed hydrogen-air flames diluted with argon. Proc. Combust. Inst. **38**(2), 2093–2100 (2021). https://doi.org/10.1016/j.proci.2020.06.124

27. Naik, S., Laurendeau, N.: Spectroscopic, calibration and RET issues for linear laser-induced fluorescence measurements of nitric oxide in high-pressure diffusion flames. Appl. Phys. B **79**, 641–651 (2004). https://doi.org/10.1007/s00340-004-1604-5

28. Šimečková, M., Jacquemart, D., Rothman, L.S., Gamache, R.R., Goldman, A.: Einstein A-coefficients and statistical weights for molecular absorption transitions in the HITRAN database. J. Quant. Spectrosc. Radiat. Transf. **98**(1), 130–155 (2006). https://doi.org/10.1016/j.jqsrt.2005.07.003

29. Gamache, R.R., Roller, C., Lopes, E., Gordon, I.E., Rothman, L.S., Polyansky, O.L., Zobov, N.F., Kyuberis, A.A., Tennyson, J., Yurchenko, S.N., Császár, A.G., Furtenbacher, T., Huang, X., Schwenke, D.W., Lee, T.J., Drouin, B.J., Tashkun, S.A., Perevalov, V.I., Kochanov, R.V.: Total internal partition sums for 166 isotopologues of 51 molecules important in planetary atmospheres: Application to HITRAN2016 and beyond. J. Quant. Spectrosc. Radiat. Transf. **203**, 70–87 (2017). https://doi.org/10.1016/j.jqsrt.2017.03.045

30. Paul, P.H., Gray, J.A., Durant, J.L., Thoman, J.W., Jr.: Collisional quenching corrections for laser-induced fluorescence measure-

ments of NO $A^2\Sigma^+$. AIAA J. **32**(8), 1670–1675 (1994). https://doi.org/10.2514/3.12158

31. Tamura, M., Berg, P.A., Harrington, J.E., Luque, J., Jeffries, J.B., Smith, G.P., Crosley, D.R.: Collisional Quenching of CH(A), OH(A), and NO(A) in low pressure hydrocarbon flames. Combust. Flame **114**(3–4), 502–514 (1998). https://doi.org/10.1016/S0010-2180(97)00324-6

32. Settersten, T.B., Patterson, B.D., Gray, J.A.: Temperature- and species-dependent quenching of NO $A^2\Sigma^+(\nu' = 0)$ probed by two-photon laser-induced fluorescence using a picosecond laser. J. Chem. Phys. **124**(23), 234308 (2006). https://doi.org/10.1063/1.2206783

33. Settersten, T.B., Patterson, B.D., Humphries, W.H., IV.: Radiative lifetimes of NO $A^2\Sigma^+(\nu' = 0, 1, 2)$ and the electronic transition moment of the $A^2\Sigma^+ - X^2\Pi$ system. J. Chem. Phys. **131**(10), 104309 (2009). https://doi.org/10.1063/1.3227520

34. Chang, A.Y., Di Rosa, M.D., Hanson, R.K.: Temperature dependence of collision broadening and shift in the NO A←X (0,0) band in the presence of argon and nitrogen. J. Quant. Spectrosc. Radiat. Transf. **47**(5), 375–390 (1992). https://doi.org/10.1016/0022-4073(92)90039-7

35. Di Rosa, M.D., Hanson, R.K.: Collision broadening and shift of NO γ(0,0) absorption lines by O_2 and H_2O at high temperatures. J. Quant. Spectrosc. Radiat. Transf. **52**(5), 515–529 (1994). https://doi.org/10.1016/0022-4073(94)90021-3

36. Almodovar, C.A., Su, W.-W., Strand, C.L., Hanson, R.K.: R-branch line intensities and temperature-dependent line broadening and shift coefficients of the nitric oxide fundamental rovibrational band. J. Quant. Spectr. Radiat. Transf. **239**, 106612 (2019). https://doi.org/10.1016/j.jqsrt.2019.106612

37. Chatelain, K.P., He, Y., Mével, R., Lacoste, D.A.: Effect of the reactor model on steady detonation modeling. Shock Waves **31**(4), 323–335 (2021). https://doi.org/10.1007/s00193-021-01022-w

38. Chi, D.J.Y., Chatelain, K.P., Lacoste, D.A.: Evaluation of detailed reaction models for the modeling of double cellular structures in gaseous nitromethane detonation. AIAA Scitech Forum, San Diego, CA, AIAA Paper 2022-2117 (2022). https://doi.org/10.2514/6.2022-2117

39. Davidenko, D., Mével, R., Dupré, G.: Numerical study of the detonation structure in rich H_2-NO_2/ N_2O_4 and very lean H_2-N_2O mixtures. Shock Waves **21**(2), 85–99 (2011). https://doi.org/10.1007/s00193-011-0297-z

40. Browne, S., Zeigler, J., Shepherd, J.E.: Numerical solution methods for shock and detonation jump conditions. Technical report FM2006-006, Graduate Aeronautical Laboratories California Institute of Technology (2008). https://shepherd.caltech.edu/EDL/publications/reprints/ShockDetonation.pdf

41. Mével, R., Javoy, S., Lafosse, F., Chaumeix, N., Dupré, G., Paillard, C.-E.: Hydrogen-nitrous oxide delay times: shock tube experimental study and kinetic modelling. Proc. Combust. Inst. **32**(1), 359–366 (2009). https://doi.org/10.1016/j.proci.2008.06.171

42. Chatelain, K.P., Alicherif, M., Rojas Chavez, S.B., Lacoste, D.A.: Nitric oxide sensitization of hydrogen detonations. AIAA Scitech 2023 Forum, National Harbor, MD, AIAA Paper 2023–1877 (2023). https://doi.org/10.2514/6.2023-1877

43. Mulla, I.A., Godard, G., Renou, B.: Instantaneous planar measurements of nitric oxide concentration in a turbulent *n*-heptane spray flame. Combust. Flame **208**, 451–471 (2019). https://doi.org/10.1016/j.combustflame.2019.07.026

44. Sahu, A.B., Mohamed, AAE-S., Panigrahy, S., Saggese, C., Patel, V., Bourque, G., Pitz, W.J., Curran, H-J.: An experimental and kinetic modeling study of NO_x sensitization on methane autoignition and oxidation. Combust. Flame **238**, 111746 (2022). https://doi.org/10.1016/j.combustflame.2021.111746